Electrocatalysis (2024) 15:42–51
https://doi.org/10.1007/s12678-023-00852-9

RESEARCH

Hydrogen-Mediated Photoelectrocatalysis with Nickel-Modified Poly(Heptazine Imides)

Sirlon F. Blaskievicz[1,2] · Ivo F. Teixeira[1,3] · Lucia H. Mascaro[1] · Mariolino Carta[4] · Neil B. McKeown[5] · Yuanzhu Zhao[2] · Frank Marken[2]

Accepted: 31 October 2023 / Published online: 11 November 2023

Abstract
Polymeric carbon nitrides (C_3N_4) are photochemically active organic semiconductors that can be produced in a wide range of structural types. Here, a poly-(heptazine imide) containing nickel single atoms (Ni-PHI) is employed for photochemical hydrogen production and is compared to the non-nickel-doped semiconductor. Film deposits are formed on a platinum disk electrode (to detect hydrogen) and a coating of the molecularly rigid polymer of intrinsic microporosity PIM-1 is applied to (i) mechanically stabilize the photo-catalyst film without impeding photocatalysis and (ii) assist in the interfacial hydrogen capture/oxygen suppression process. In the presence of hole quenchers such as methanol or ethanol, anodic photocurrents linked to hydrogen production/oxidation are observed. A comparison with an experiment on glassy carbon confirms the formation of interfacial hydrogen as a mediator. The effects of hole quencher concentration are evaluated. The system Pt/Ni-PHI/PIM-1 is employed in a single-compartment photo-fuel cell.

Introduction

Studies involving clean energy transformations are driven by a tangible global energy transition and by ameliorating environmental pollution [1]. New materials that can be employed in energy systems (e.g. photoreactors, fuel cells, or batteries) help address the demand for renewable energy [2]. Photochemical reactions based on small molecule oxidation, such as the methanol oxidation reaction (here as a model for biomass oxidation), can be employed to release hydrogen for the future development of greener energy devices. Commonly, platinum (Pt) plays a fundamental part in this process given its high catalytic activity for hydrogen evolution. However, due to the high price and poor sustainability, it is necessary to use approaches that replace Pt, for example with Ni, combined with an organic photocatalyst and using a light source as energy input into the system.

Promising photocatalyst materials today are carbon nitrides (C_3N_4). These nonmetallic semiconductors, essentially made of carbon and nitrogen atoms, can be synthesized by low-cost methods, e.g. melamine thermo-polymerization in a medium containing molten alkali metal salts [3]. This method of synthesis leads to an organized (highly graphitic) and homogeneous structure of a carbon nitride as poly(heptazine imide) or PHI. The pyridinic and imide nitrogens of the PHI offer possibilities for the coordination of transition metals as single atoms between the heptazine rings. After the synthesis, the alkali metal ions employed stay coordinated, and allow by a simple cation exchange method, the introduction of other metal cations such as Ni(II) [4] or Fe(II) [5, 6]. As reported by Pérez-Ramírez et al. [7], replacing cations in PHI with Pd^{2+} leads to palladium single-atoms coordinated to PHI (Pd-PHI) to catalyze Suzuki coupling reactions, achieving an efficiency comparable to that of common Pd(0) homogeneous catalysts. Thus, the immobilization of atomically dispersed transition metals into graphitic carbon nitrides leads to areas of potential applications, such as green energy generation, solar fuels production/conversion (hydrogen), and photocatalytic biomass transformation.

Alternative reaction mechanisms in photoelectrochemistry involving hydrogen as a mediator (instead of electrons/holes) have been reported for platinum [8, 9] and for palladium [10, 11] electrodes or membranes. Here, hydrogen is employed as an intermediate to shuttle electrons to the electrode surface. This process is facilitated by intrinsically microporous polymer materials (PIMs) such as PIM-1 [12, 13]. PIM-1 has a large Brunauer-Emmett-Teller (BET) surface area (in the range of 600–900 $m^2\ g^{-1}$) and microporous channels typically with a

Lucia H. Mascaro conceived and supervised work on this project. She is involved in all aspects of developing and reporting this work.

Extended author information available on the last page of the article

Graphical Abstract

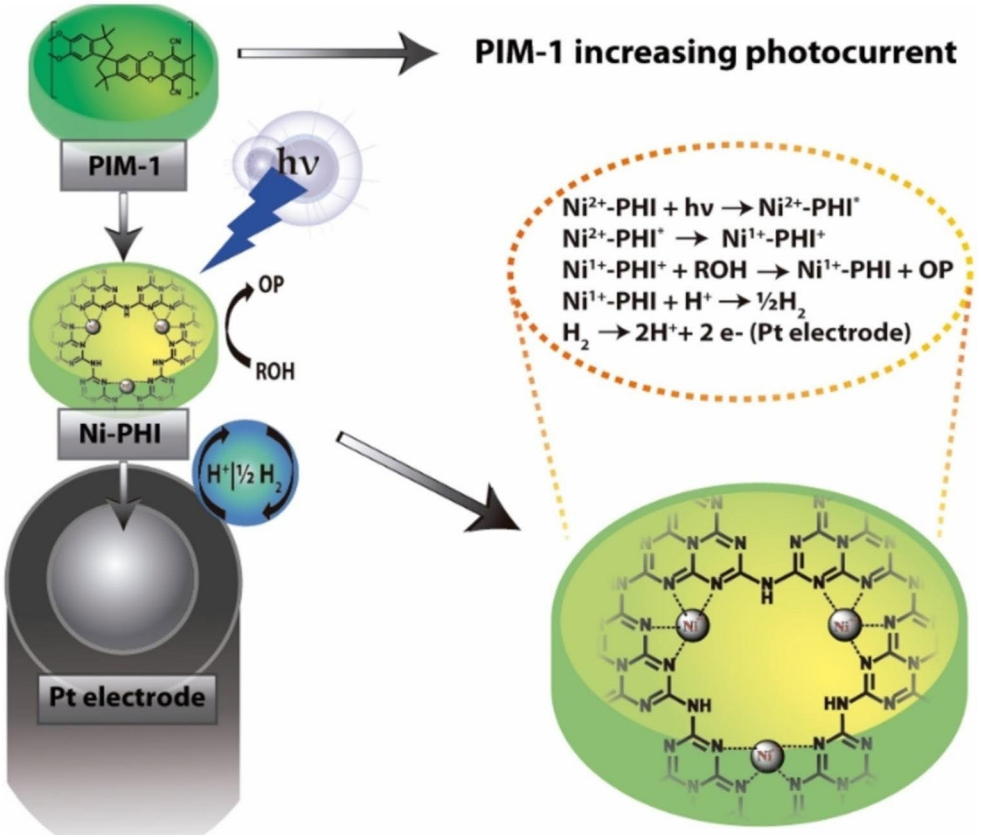

Keywords Biomass · Photofuel cell · Photocatalysis · Hydrogen · Intrinsic Microporosity

diameter of 1 nm [14]. PIM-1 has been studied in gas adsorption and permeation [14], and it has been employed in electrochemistry [15], photoelectrochemistry [9], batteries [16], and redox flow cell systems [17].

In this study, a PHI-based photocatalyst containing atomically dispersed nickel (Ni-PHI) is immobilized with PIM-1 at the surface of a platinum disk electrode to demonstrate photohydrogen production. Figure 1 shows the experimental configuration with PIM-1 and photocatalyst Ni-PHI immobilized on the surface of a glassy carbon or platinum disk electrode as the working electrode (WE). A LED light source is deployed to provide light pulses during voltammetry experiments performed with a potentiostatically controlled, three-electrode cell (working electrode - WE, reference electrode - RE, and counter electrode - CE). For the photofuel cell, a two-electrode system was employed, with a platinum foil as the counter electrode.

In this preliminary study of photoelectrochemical reactions with PIM-1 host film coatings on Ni-PHI photocatalyst, mechanical stabilization and an enhancement in the photoelectrochemical response to hydrogen were observed, when compared to the uncoated films. A phosphate buffer inhibitory effect in the nickel-catalyzed process is investigated. The role of ambient oxygen is discussed. A mechanism is tentatively assigned based on the photochemical hydrogen production coupled to re-oxidation at the platinum electrode.

Experimental

Reagents

Chemicals were purchased from Fisher Scientific or Sigma-Aldrich and used without further purification. Aqueous solutions were prepared under ambient conditions by using ultrapure water (resistivity of 18.2 MOhm cm at 22 °C). Argon (Pureshield, BOC, UK) was employed to de-aerate solutions where indicated. PIM-1 was prepared according to the literature [18, 19], and a stock solution of PIM-1 (1 mg/mL) was prepared in chloroform. The photocatalyst Na-PHI was obtained by adopting a literature methodology [3]. In brief, 1 g of melamine (99%, Sigma-Aldrich) ground with 10 g of NaCl (99%, Sigma-Aldrich) was heated in an oven under constant nitrogen atmospheric (São Carlos Química, BR) flow (5 L min^{-1}) to 600 °C for 4 h with a heating rate of 2.3 °C min^{-1}.

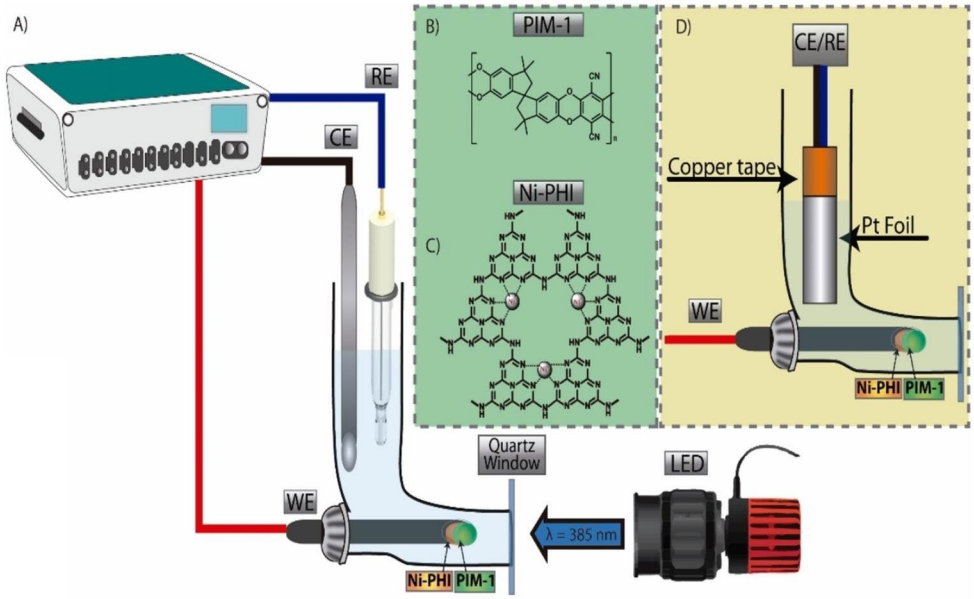

Fig. 1 **(A)** Experimental setup for photoelectrochemical investigation of Ni-PHI coated with PIM-1; Molecular structure of **(B)** PIM-1 and **(C)** Ni-PHI; **(D)** Experimental setup of the two electrode photofuel cell

For Ni-PHI synthesis, the Ni^{2+} single atom sites were introduced in the Na-PHI structure by cation exchange [6], where the Ni^{2+} cations replace Na^{+} in the carbon nitride structure. Na-PHI (0.1 g) was suspended with 1.6 mmol of $NiCl_2$ (98%, Sigma-Aldrich) in 2.0 mL of water by sonication for 30 min. Then the sample was filtered, extensively washed with deionized water and acetone (99.5%, Fisher Scientific), and dried overnight in an oven at 60 °C.

Instrumentation

Diffuse reflectance UV-vis spectroscopy (DRUV-vis) was performed in a Cary 5G® spectrometer. To investigate the structure and morphology of Ni-PHI, high-angle annular dark-field imaging scanning transmission electron microscopy (HAADF-STEM) experiments were performed. For image acquisition, the sample was sonicated in isopropanol for 10 min to give a suspension. This was dropped onto an Au sample grid. Images were collected at a probe convergence semi-angle of 25 mrad, using a double Cs corrected JEOL JEM-ARM200F (S)TEM operated at 80 kV equipped with a cold field emission gun.

Electrochemical experiments were performed with an Autolab PGSTAT (Metrohm, UK) controlling a three-electrode cell, using a platinum or glassy carbon disk (BASi, UK) with 3 mm diameter as working electrode, a saturated calomel (SCE) as reference electrode, and a platinum wire counter electrode. Before use, the working electrode surfaces (platinum or glassy carbon) were carefully polished with alumina powder (α-Al_2O_3) 0.3 µm, rinsed with distilled water, and cleaned by sonication for 10 min, in an ethanol/water 1:1 (v/v) solution. The cell was illuminated with a power LED (λ=385 nm, approx. 100 mW cm^{-2} calibrated at approx. 1.8 cm distance, Thorlabs, UK). It was assumed that the quartz plate and solution phase do not significantly absorb at 385 nm. After use, the cell was rinsed with isopropanol and with pure water. Chronopotentiometry experiments were performed in an indirect photo-fuel cell, where the counter/reference electrode was a platinum foil (1×3 cm^2). The working electrode was prepared by deposition of 10 µL of Ni-PHI (suspension in isopropanol 1 mg mL^{-1}) and coating with 10 µL of PIM-1. Therefore, the mass loading of photocatalyst was fixed at 10 µg on a 7×10^{-6} m^2 electrode area. The effects of varying this mass loading could be significant but have so far not been investigated. All experiments were performed in ambient air if not stated otherwise.

Results and Discussion

Characterization of Nickel Single Atoms in Ni-PHI

The Ni-PHI photocatalyst was characterized in a previous study [20]. In brief, the XRD analysis showed that this sample possesses high crystallinity. Data from infrared spectroscopy exhibited typical absorption bands of the PHI structure, as well as a blueshift, observed in the CN modes when compared to the unmodified sample (Na-PHI). This was strong evidence of nickel coordination. Furthermore, the presence of isolated sites was indicated by diffuse reflectance infrared Fourier transform spectroscopy (DRIFTS) with carbon monoxide (CO) as a probe molecule. The analysis showed only peaks related to linearly adsorbed CO (2040 and 2179 cm^{-1}), while peaks related to multi-site coordinated CO (bridged bonded) from 1900 to 2000 cm^{-1} were absent. Figure 2 A presents the diffuse-reflectance UV-vis (DRUV-vis) spectra for the Na-PHI and Ni-PHI, where both samples exhibit bands in ~430 nm assigned to the π-π* transitions, that resemble the semiconductor band gap onset [21]. From the linear extrapolation of the Tauc plot curves

(presented in the inset of the DRUV-vis graph), the band gap obtained for Na-PHI was 2.85 eV, while Ni-PHI gave a slight redshift to 2.81 eV presumably due to the nickel coordination.

In the HAADF-STEM images of Ni-PHI, presented in Fig. 2B, it is possible to observe highly dispersed bright spots, concerning the nickel species, since the contrast between Ni, N, and C elements are different [22]. In Fig. 2 agglomerates of nickel, i.e. clusters or nanoparticles, are not identified, indicating that nickel is present only at single atom sites. The covalent coordination in the pyridinic nitrogen allows not only a homogeneous distribution of the nickel species but also a high stability towards leaching. Furthermore, highly dispersed species imply that nickel acts as isolated sites for catalytic reactions.

Effects of Nickel in Ni-PHI for Methanol Photoelectro-Oxidation

Initially, a dispersion was prepared by mixing equal proportions, in mass, of PIM-1 with the photocatalyst (Na-PHI or Ni-PHI), in chloroform. Next, 10 μg of the prepared suspension was deposited over a 3 mm diameter platinum electrode and investigated in methanol photo-oxidation experiments. Figure 3 shows cyclic voltammetry with pulsed light (LED, 385 nm, approx. 100 mW cm^{-2}, 2 s on and 1 s off), in 10 mmol L^{-1} of methanol in a buffered solution (pH 7, KH_2PO_4, 0.02 mol L^{-1}), with KCl (0.1 mol L^{-1}) as supporting electrolyte. For the suspension deposit, no significant photocurrent was observed. On the other hand, when first depositing a layer of the carbon nitride (10 μg), then coating with 10 μg of PIM-1 (or Ni-PHI/PIM-1), clear oxidation photocurrents result at 0.0 V vs. SCE for both Na-PHI and Ni-PHI. Note that the presence of K^+ in the electrolyte could have caused some cation exchange for Na-PHI, but not for Ni-PHI. Photocurrents are observed as transients with a rise time of typically 1 s probably associated mainly with hydrogen (H_2) reaching/diffusing towards the platinum electrode surface. Effects from quencher diffusion are unlikely under these conditions. In comparison to uncoated materials, the photocurrent was doubled after coating with PIM-1. The improved results with the coating instead of the mixture indicate that it is better to have the photocatalyst compact close to the electrode, with better mechanical stability in the presence of the coating. Loss of the carbon nitride deposit was observed when bare samples were in direct contact with the solution. Furthermore, in addition to mechanical stability, the main hypothesis for the increase in photocurrent response is that the PIM-1 film can capture hydrogen (whilst suppressing oxygen transport to the electrode) and mitigate the nucleation of gas bubbles in the active photocatalyst sites [9].

To investigate the photocurrent enhancement, higher concentrations of methanol were investigated as presented in the chronoamperometry data obtained at 0 V vs. SCE, under chopped illumination (10 s on/10 seconds off) as shown in Fig. 4. In the system Ni-PHI/PIM-1 (Fig. 4A), with up to 40 mmol L^{-1} methanol, the photocurrent still increased with saturation close to ~18 μA for 50 mmol L^{-1} methanol. In comparison, with Na-PHI (Fig. 4B) it is possible to observe that the photocurrent reaches only a lower current plateau. This difference can be explained by the presence of Ni^{2+} species, which is known to be a good electrocatalyst [23] and able to generate hydrogen. The chronoamperometry also allowed us to evaluate the stability of the system. After 10 min of measurement, the photocurrent did not change significantly, which indicates that the coating with PIM-1 prevents the loss of the photocatalyst activity. The nickel catalyst was not poisoned or depleted during photocatalysis [24].

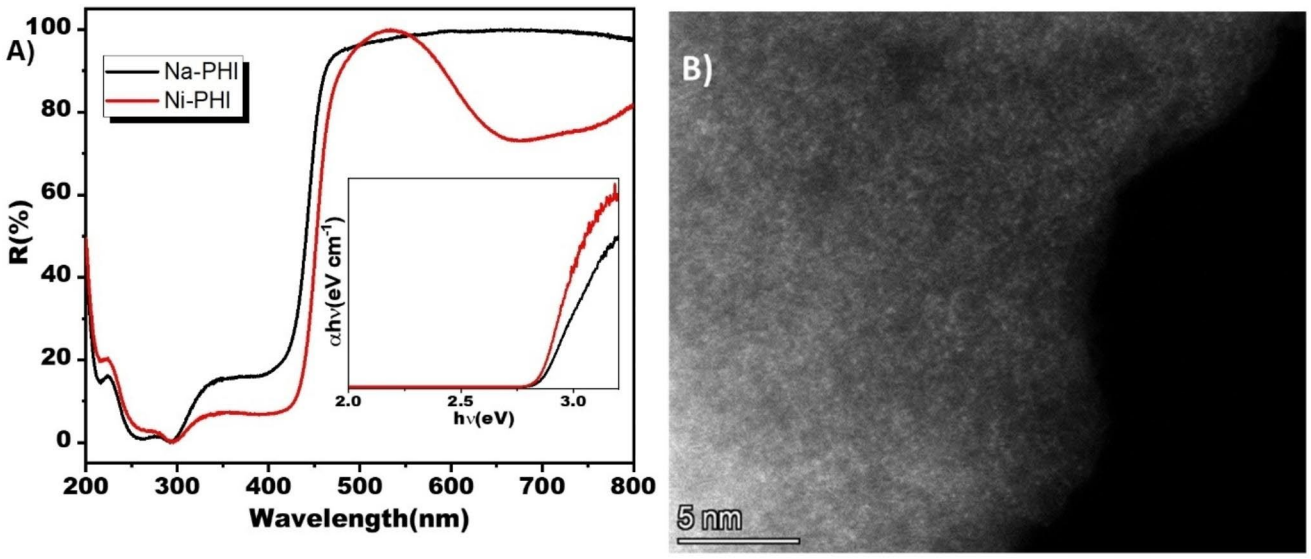

Fig. 2 **(A)** DRUV-vis and Tauc plot (inset) of Na-PHI and Ni-PHI samples, and **(B)** STEM-HAADF image of Ni-PHI.

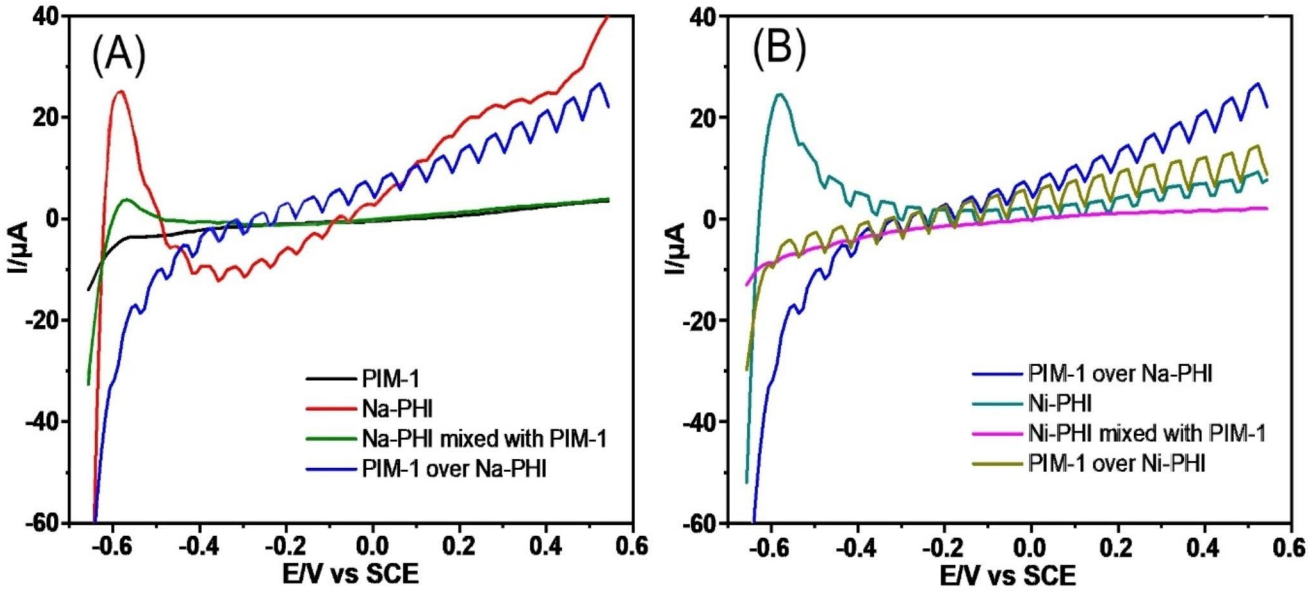

Fig. 3 Linear sweep voltammetry (scan rate 20 mVs^{-1}) under chopped illumination using a 385 nm LED (2 s on 1 s off), 10 mM methanol, 0.1 M KCl, 20 mM KH_2PO_4 buffer pH 7 for **(A)** Na-PHI and the combinations with PIM-1 and **(B)** Ni-PHI and the combinations with PIM-1

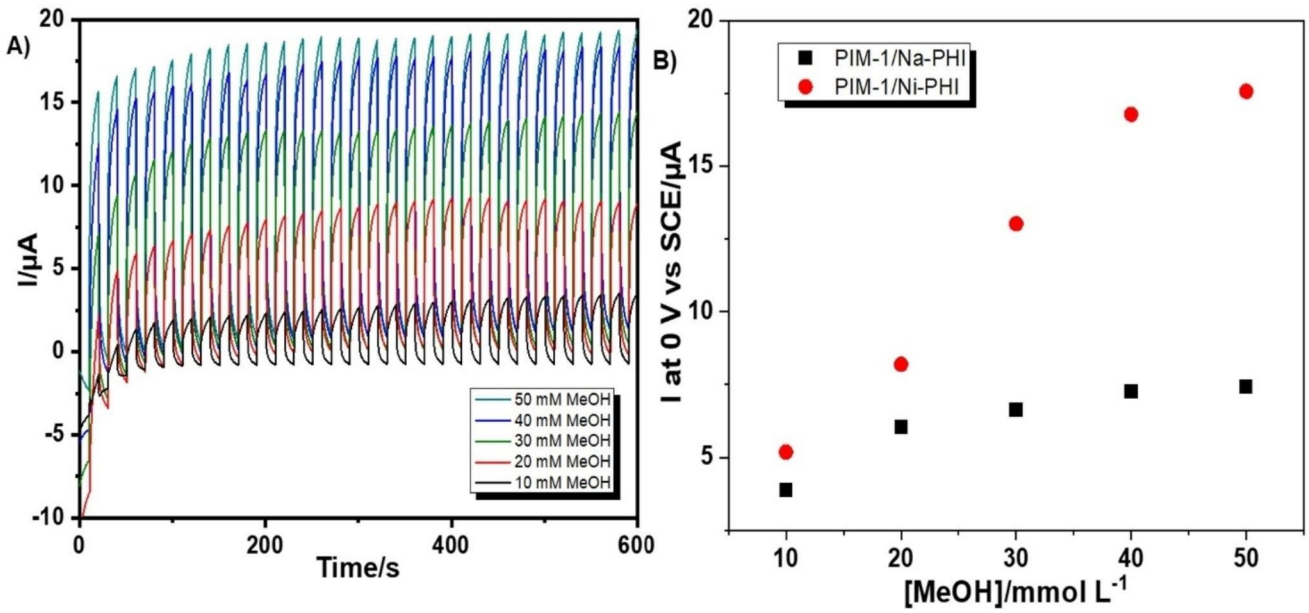

Fig. 4 **(A)** Chronoamperometry at 0 V vs. SCE for 10 μg of PIM-1 over 10 μg of Ni-PHI; **(B)** Photocurrent at 0 V vs. SCE for 10 μg of PIM-1 over 10 μg of Na-PHI and Ni-PHI with different methanol concentrations

Next, the photocurrent responses were investigated in unbuffered media to elucidate the effects of phosphate anion binding. The black lines in Fig. 5 refer to the baseline signal without PIM-1 when applying pulses of light (LED, 385 nm, approx. 100 mW cm^{-2}, 2 s on and 1 s off). Generally, the anodic photocurrent was higher than that observed in the presence of phosphate buffer. The same was observed for the coated samples with 10 (blue lines) or 50 (yellow lines) mmol L^{-1} methanol, whereby Ni-PHI/PIM-1 presented a photocurrent ~ 30 μA at 0 V vs. SCE, almost double that in the buffered media. This suggests that hydrogen is being generated from the photocatalyst and reoxidized at the Pt electrode. Once phosphate anions adsorb to the nickel sites, competition for the active sites with hydrogen evolution may somewhat lower hydrogen production [25, 26]. The assumption of hydrogen oxidation at the platinum electrode is supported when investigating the PIM-1/Ni-PHI system under the same conditions but deposited onto glassy carbon (GC) (Fig. 5C). A much lower photocurrent suggests

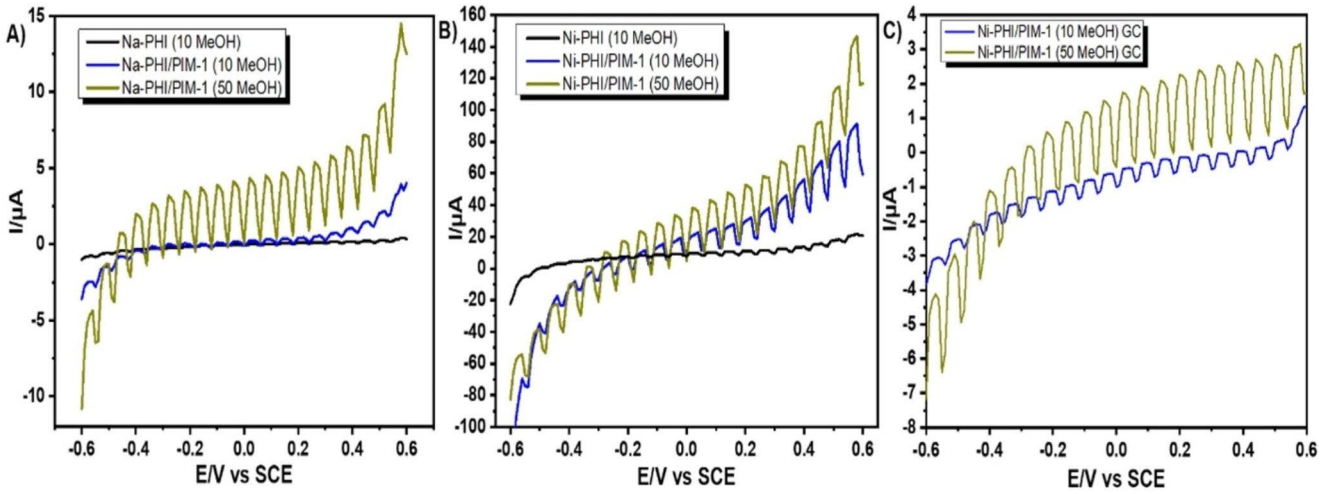

Fig. 5 Linear sweep voltammetry (scan rate 20 mV s^{-1}) under pulsed illumination using a 385 nm LED (2 s on and 1 s off), with 10 (black and blue lines) and 50 (golden lines) mmol L^{-1} methanol in KCl 0.1 mol L^{-1}, with and without 10 μg of PIM-1 on **(A)** 10 μg of Na-PHI/PIM-1 on Pt electrode, **(B)** 10 μg of Ni-PHI/PIM-1 on Pt electrode, and **(C)** Ni-PHI/PIM-1 over GC electrode

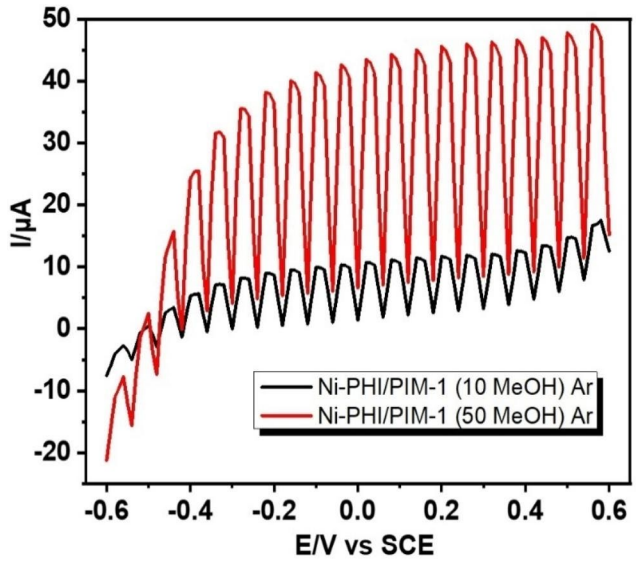

Fig. 6 Linear sweep voltammetry (scan rate 20 mV s^{-1}) under pulsed illumination using a 385 nm LED (2 s on and 1 s off), with 10 (black line) and 50 (red line) mmol L^{-1} methanol in KCl 0.1 mol L^{-1}, with 10 μg of PIM-1 on 10 μg of Ni-PHI over Pt electrode, under argon atmosphere

that the Pt electrode is necessary for hydrogen oxidation. For a concentration of 50 mmol L^{-1} of methanol, the photocurrent measured over GC was ~2 μA at 0 V vs. SCE, while at the same potential, over Pt, this value was ~30 μA.

The effect of argon deaeration on the photocurrents is significant. Figure 6 shows that for 10 mM and 50 mM methanol, further enhancements in photocurrents are observed. In argon, the photocurrent increases from approx. 18 μA (in Fig. 4) to 45 μA in the presence of 50 mM methanol (Fig. 6). This corresponds to a mass activity of 45 μA per 10 μg photocatalyst or a hydrogen flux of 0.2 nmol s^{-1} per 10 μg photocatalyst, although further study will be required to more quantitatively explore the effect of mass loading on hydrogen production. Oxygen is a quencher for H_2 at the Pt electrode and clearly interferes. In practice, photo-fuel cells argon deaeration is an unwanted complication and a somewhat lower hydrogen production and photocurrent have to be accepted. Further optimization of photocatalyst loading and photocatalyst to PIM-1 ratio will be possible.

Effects of Nickel on Ethanol Photo-Oxidation

For ethanol oxidation, the optimized conditions for methanol (10 μg of PIM-1 over 10 μg of Na or Ni-PHI) were employed and processes were evaluated for 10 and 50 mmol L^{-1} of ethanol. The photocurrents are presented in Fig. 7. The system behaves similarly to the case of methanol as a quencher. The nickel-containing sample performed better than that of Na-PHI, presenting respectively a photocurrent of 7.8 and 1.2 μA at 0 V vs. SCE for 50 mmol L^{-1} of ethanol. The anodic photocurrents obtained with ethanol were somewhat lower than those for methanol, possibly due to intermediates in the complex reaction. The photocatalyst (Na-PHI or Ni-PHI) is oxidizing ethanol associated with hydrogen generation, which is then captured by the PIM-1 film.

Based on these results, the proposed pathway for the oxidation of alcohols (ROH) in the Pt/Ni-PHI/PIM-1 system is presented in the following sequence of steps: photoexcitation of the PHI structure (Eq. 1), charge separation reducing the oxidation state of nickel ions (Eq. 2), hole quenching with the oxidation of ROH to oxidation products (OP) (Eq. 3), evolution (Eq. 4) and, consumption (Eq. 5) of hydrogen in the platinum electrode.

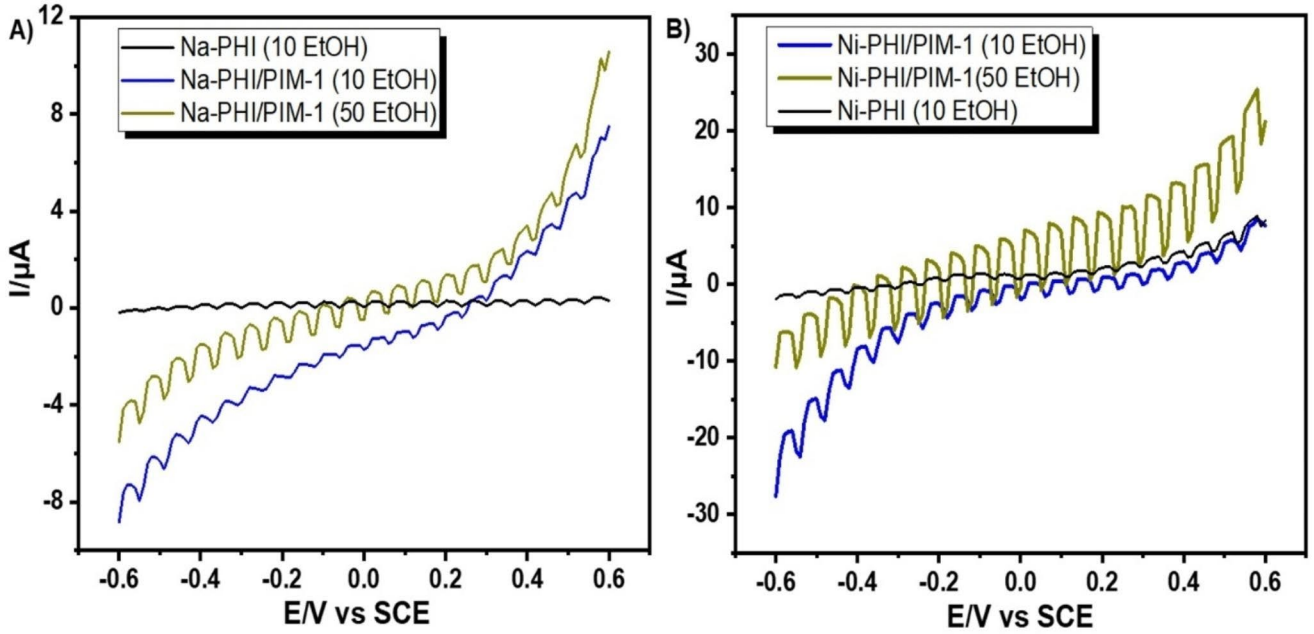

Fig. 7 Linear sweep voltammetry (scan arte 20 mV s^{-1}) under chopped illumination using a 385 nm LED (2 s on and 1 s off), 0.1 M KCl, 20 mM KH_2PO_4 buffer pH 7 for **(A)** Na-PHI/PIM-1, **(B)** Ni-PHI/PIM-1.

$$\mathbf{Ni^{2+} - PHI} + h\nu \rightarrow \mathbf{Ni^{2+} - PHI^{*}} \quad (1)$$

$$\mathbf{Ni^{2+} - PHI^{*}} \rightarrow \mathbf{Ni^{+} - PHI^{+}} \quad (2)$$

$$\mathbf{Ni^{+} - PHI^{+}} + \mathbf{ROH} \rightarrow \mathbf{Ni^{+} - PHI} + \mathbf{OP} \quad (3)$$

$$\mathbf{Ni^{+} - PHI} + \mathbf{H^{+}} \rightarrow \tfrac{1}{2}\,\mathbf{H_2} \quad (4)$$

$$\mathbf{H_2} \rightarrow \mathbf{2\ H^{+} + 2\ e^{-}\ (Pt\ electrode)} \quad (5)$$

Single Compartment Photo-Fuel Cell Processes with Ni-PHI

Ni-PHI/PIM-1 was employed as a working electrode in an exploratory fuel photocell, using a platinum foil as a counter/reference electrode defined by ambient oxygen in the system (Fig. 1). The same compartment contains the fuel for both anode and cathode. First, the open circuit potential (OCP) of the system was measured for the lowest concentration (10 mmol L^{-1}), and for the concentration where photocurrent saturation occurs (50 mmol L^{-1}) with continuous light irradiation (λ = 385 nm) for 950 s. The illuminated OCP value was approximately 0.58 V for 10 mmol L^{-1} of methanol and 0.65 V for 50 mmol L^{-1} methanol (Fig. 8A). In the presence of ethanol (Fig. 8B), the OCP values were 0.54 and 0.57 V for 10 and 50 mmol L^{-1}, respectively, in agreement with the lower efficiency of ethanol as a hole quencher.

Subsequently, cyclic voltammetry measurements were carried out starting at OCP with a scan rate of 1 mV s^{-1} to give information about the fuel cell power generation. From the potential sweep, it was possible to construct the cell power graph (P = E × i), presented in Fig. 8C and D. In the measurements with methanol (Fig. 8C), it is noteworthy that there is power generation in wide a range of 0 to ~0.5 V. The system reaches maximum powers of 1.3 μW (for 10 mmol L^{-1} of methanol) and 2.1 μW (50 mmol L^{-1} of methanol) at 0.4 V. These values are comparable to other membrane-less fuel cells found in the literature [27, 28]. For ethanol (Fig. 8B), the powers were 0.4 μW and 0.9 μW at 0.3 V for 10 and 50 mmol L^{-1}, respectively. In the future, the effects of convection, quencher concentration and type, and light intensity could provide further improvements.

Conclusions and Outlook

The present study showed that the presence of Ni^{2+} single sites sharply increases the photoelectrochemical (hydrogen-mediated) response for both methanol and ethanol oxidation when compared to the PHI photocatalyst without the transition metal. The unique microporous environment in PIM-1 improved the mechanical stability of the photocatalyst film and added to the control of the diffusion of the reactants/oxygen towards the photocatalysts. The microporous PIM-1 affects the transport of reactants to/ products away from the photochemical reaction zone and it may affect the light intensity at the location of the photocatalyst. Effects will depend on the reaction conditions and the interaction of reactants with the microporous

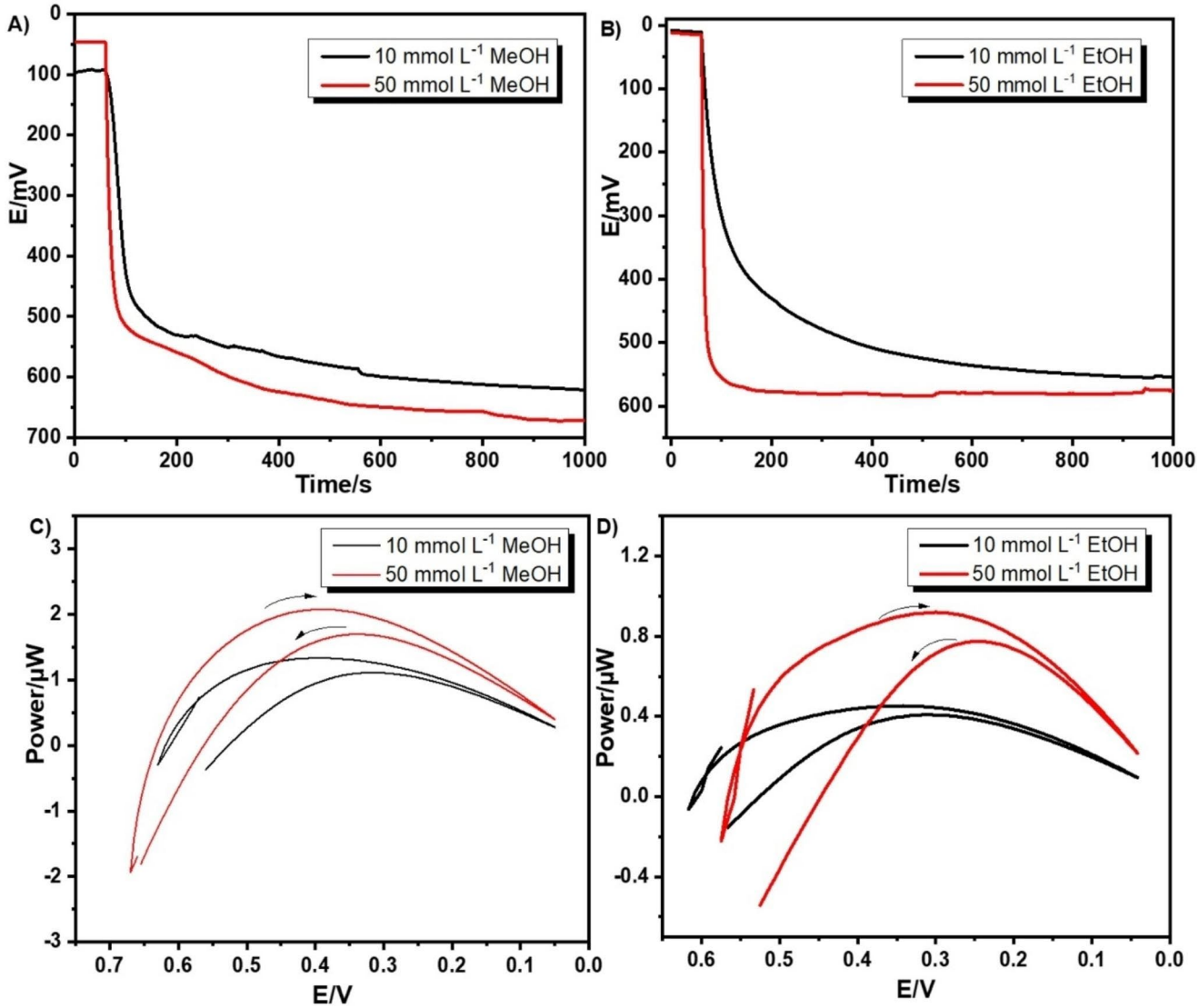

Fig. 8 Chronopotentiometry in OCP for a two-electrode photocell with 385 nm LED light with **(A)** methanol, **(B)** ethanol; and power (current × voltage) voltammograms (scan rate 1 mV s^{-1}) as a function of the voltage of the fuel photocell of the PIM-1/Ni-PHI system obtained for **(C)** methanol and **(D)** ethanol

host. Further quantitative study is required to determine the local concentration and diffusivity of hydrogen gas under these conditions.

The photocatalyst performance is linked to H_2 generation by the quencher oxidation followed by hydrogen trapping by PIM-1 and hydrogen oxidation at the platinum electrode. Transport rates of gases such as hydrogen and oxygen in the glassy PIM-1 structure are low compared to those in bulk solution, but further study is necessary. Further effects from the PIM-1 host structure on the photocatalytic reaction and the electrochemical process need to be investigated.

The architecture Pt/Ni-PHI/PIM-1 was applied in a two-electrode fuel cell, enabling power generation in a wide range of potentials. In the future, the efficiency of this type of hydrogen-mediated process needs to be improved for example by exploring a wider range of biomass quenchers and by limiting the energy consumption by light. Platinum in the cathode can be removed and replaced by sustainable catalyst alternatives or by membranes (e.g. hydrogen-permeating Teflon membranes [29]). Furthermore, carbon nitrides have been shown to be piezocatalytic, which could provide a future pathway away from light activation towards sound/mechano activation. Generally, photocatalyst films in PIM hosts could be of wider use in photocatalysis and photoelectrocatalysis. PIMs provide a unique molecularly rigid microporous environment for photocatalysts to be immobilized at surfaces and surrounded by the aqueous electrolyte phase.

Authors' contributions S.F.B. carried out experiments, processed data, and wrote the draft manuscript. I.F.T. and L.H.M. provided supervision and discussion. M.C. and N.B.M. provided supervision and support

with polymer materials. Y.Z. assisted in data analysis and manuscript preparation. F.M. provided supervision and discussion. All authors reviewed the manuscript.

Funding S.F.B. thanks to the financial support of the CAPES Foundation for a sandwich doctorate scholarship (CAPES-PRINT Process 88887.465542/2019-00). L.H.M. thanks to FAPESP (2017/11986-5, 2020/14741-6, 2014/50249-8). Y.Z. (201809350006) is grateful to the China Scholarship Council for a PhD scholarship.

Data Availability Data and materials are available from the authors.

Declarations

Ethical Approval Ethical approval was obtained at the departmental level.

Competing interests The authors declare no competing interests.

References

1. J. Xiao, Y. Xu, Y. Xia, J. Xi, S. Wang, Ultra-small Fe_2N nanocrystals embedded into mesoporous nitrogen-doped graphitic carbon spheres as a highly active, stable, and methanol-tolerant electrocatalyst for the oxygen reduction reaction. Nano Energy. **24**, 121–129 (2016). https://doi.org/10.1016/j.nanoen.2016.04.026
2. J.F. Chang, L.G. Feng, C.P. Liu, W. Xing, X.L. Hu, Ni_2P enhances the activity and durability of the pt anode catalyst in direct methanol fuel cells. Energy Environm Sci. **7**, 1628–1632 (2014). https://doi.org/10.1039/c4ee00100a
3. Z. Chen, A. Savateev, S. Pronkin, V. Papaefthimiou, C. Wolff, M.G. Willinger, E. Willinger, D. Neher, M. Antonietti, Dontsova. The easier the better preparation of efficient photocatalysts-metastable poly(heptazine imide) salts. Adv. Mater. **29**, 1700555 (2017). https://doi.org/10.1002/adma.201700555
4. M.A.R. da Silva, G.F.S.R. Rocha, G.A.A. Diab, C.S. Cunha, V.G.S. Pastana, I.F. Teixeira, Simple and straightforward method to prepare highly dispersed ni sites for selective nitrobenzene coupling to Azo/Azoxy compounds. Chem Eng. J. **460** (2023). https://doi.org/10.1016/j.cej.2022.141068
5. M.A.R. da Silva, I.F. Silva, Q. Xue, B.T.W. Lo, N.V. Tarakina, B.N. Nunes, P. Adler, S.K. Sahoo, D.W. Bahnemann, N. López-Salas, A. Savateev, C. Ribeiro, T.D. Kühne, M. Antonietti, I.F. Teixeira, Sustainable oxidation catalysis supported by light: Fe-poly (heptazine imide) as a heterogeneous single-atom photocatalyst. Appl. Catal. B Environm. **304**, 120965 (2022). https://doi.org/10.1016/j.apcatb.2021.120965
6. F.M. Colombari, M.A.R. da Silva, M.S. Homsi, B.R.L. de Souza, M. Araujo, J.L. Francisco, G.T.S.T. da Silva, I.F. Silva, A.F. de Moura, I.F. Teixeira, Graphitic carbon nitrides as platforms for single-atom photocatalysis. Faraday Discuss. **227**, 306–320 (2021). https://doi.org/10.1039/c9fd00112c
7. Z. Chen, E. Vorobyeva, S. Mitchell, E. Fako, M.A. Ortuño, N. López, S.M. Collins, P.A. Midgley, S. Richard, G. Vilé, A heterogeneous single-atom palladium catalyst surpassing homogeneous systems for Suzuki coupling. Nat. Nanotechnol. **13**, 702–704 (2018). https://doi.org/10.1038/s41565-018-0167-2
8. I. Ledezma-Yanez, O. Díaz-Morales, M.C. Figueiredo, M.T. Koper, Hydrogen oxidation and hydrogen evolution on a platinum electrode in acetonitrile. ChemElectroChem. **2**, 1612–1614 (2015). https://doi.org/10.1002/celc.201500341
9. Y. Zhao, N.A. Al Abass, R. Malpass-Evans, M. Carta, N.B. Mckeown, E. Madrid, P.J. Fletcher, F. Marken, Photoelectrochemistry of immobilised Pt@g-C_3N_4 mediated by hydrogen and enhanced by a polymer of intrinsic microporosity PIM-1. Electrochem. Commun. **103**, 1–6 (2019). https://doi.org/10.1016/j.elecom.2019.04.006
10. A. Mahajan, S.K. Bhattacharya, S. Rochat, A.D. Burrows, P.J. Fletcher, Y. Rong, A.B. Dalton, N.B. McKeown, F. Marken, Polymer of intrinsic microporosity (PIM-7) coating affects triphasic palladium electrocatalysis. ChemElectroChem. **16**, 4307–4317 (2019). https://doi.org/10.1002/celc.201801359
11. Y. Zhao, J. Dobson, C. Harabajiu, E. Madrid, T. Kanyanee, C. Lyall, S. Reeksting, M. Carta, N.B. McKeown, L. Torrente-Murcianog, K. Black, F. Marken, Indirect photo-electrochemical detection of carbohydrates with Pt@g-C_3N_4 immobilised into a polymer of intrinsic microporosity (PIM-1) and attached to a palladium hydrogen capture membrane. Bioelectrochem. **134**, 107499 (2020). https://doi.org/10.1016/j.bioelechem.2020.107499
12. L.N. Wang, Y.Z. Zhao, B.B. Fan, M. Carta, R. Malpass-Evans, N.B. McKeown, F. Marken, Polymer of intrinsic microporosity (PIM) films and membranes in electrochemical energy storage and conversion: a mini-review. Electrochem. Commun. **118**, 106798 (2020). https://doi.org/10.1016/j.elecom.2020.106798
13. E. Madrid, N.B. McKeown, Innovative methods in electrochemistry based on polymers of intrinsic microporosity. Curr Opin. Electrochem. **10**, 61–66 (2018). https://doi.org/10.1016/j.coelec.2018.04.008
14. P.M. Budd, N.B. Mckeown, B.S. Ghanem, K.J. Msayib, D. Fritsch, L. Starannikova, N. Belov, O. Sanfirova, Y. Yampolskii, V. Shantarovich, Gas permeation parameters and other physicochemical properties of a polymer of intrinsic microporosity: polybenzodioxane PIM-1. J. Membrane Sci. **325**, 851–860 (2008). https://doi.org/10.1016/j.memsci.2008.09.010
15. E. Madrid, J.P. Lowe, K.J. Msayib, N.B. McKeown, Q.L. McKeown, G.A. Song, T. Attard, F. Duren, Marken, Triphasic nature of polymers of intrinsic microporosity induces storage and catalysis effects in hydrogen and oxygen reactivity at electrode surfaces. ChemElectroChem. **6**, 252–258 (2019). https://doi.org/10.1002/celc.201800177
16. Q. Yang, W. Li, C. Dong, Y. Ma, Y. Yin, Q. Wu, Z. Xu, W. Ma, C. Fan, K. Sun, PIM-1 as an artificial solid electrolyte interphase for stable lithium metal anode in high-performance batteries. J. Energy Chem. **42**, 83–90 (2020). https://doi.org/10.1016/j.jechem.2019.06.012
17. I.S. Chae, T. Luo, G.H. Moon, W. Ogieglo, Y.S. Kang, M. Wessling, Ultra-high proton/vanadium selectivity for hydrophobic polymer membranes with intrinsic nanopores for redox flow Battery. Adv. Energy Mater. **6**, 1600517 (2016). https://doi.org/10.1002/aenm.201600517
18. P.M. Budd, E.S. Elabas, B.S. Ghanem, S. Makhseed, N.B. McKeown, K.J. Msayib, C.E. Tattershall, D. Wang, Solution-processed, organophilic membrane derived from a polymer of

intrinsic microporosity. Adv. Mater. **16**, 456–459 (2004). https://doi.org/10.1002/adma.200306053
19. P.M. Budd, B.S. Ghanem, S. Makhseed, N.B. McKeown, K.J. Msayib, C.E. Tattershall, Polymers of intrinsic microporosity (PIMs): robust, solution-processable, organic nanoporous materials. Chem. Commun. 230–231 (2004). https://doi.org/10.1039/b311764b
20. S.F. Blaskievicz, H.L.S. Santos, I.F. Teixeira, J.L. Bott-Neto, P.S. Fernández, L.H. Mascaro, Nickel-modified polymeric carbon nitride for improving TiO_2-based photoanode: photoelectrocatalytical evaluation and mechanistical insights. Mater. Today Nano. **18**, 100192 (2022). https://doi.org/10.1016/j.mtnano.2022.100192
21. A.B. Jorge, D.J. Martin, M.T. Dhanoa, A.S. Rahman, N. Makwana, J. Tang, A. Sella, F. Cora, S. Firth, J.A. Darr, P.F. McMillan, H_2 and O_2 evolution from water half-splitting reactions by graphitic carbon nitride materials. J. Phys. Chem. C **117**, 7178–7185 (2013). https://doi.org/10.1021/jp4009338
22. S. Shen, C. Han, B. Wang, Y. Wang, Self-supported nickel single atoms overwhelming the concomitant nickel nanoparticles enable efficient and selective CO_2 electroreduction. Adv. Mater. Interfaces. **8**, 2101542 (2021). https://doi.org/10.1002/admi.202101542
23. X.P. Wang, S.B. Xi, W.S.V. Lee, P.R. Huang, P. Cui, L. Zhao, W.C. Hao, X.S. Zhao, Z.B. Wang, H.J. Wu, H. Wang, C.Z. Diao, A. Borgna, Y.H. Du, Z.G. Yu, S. Pennycook, J.M. Xue, Materializing efficient methanol oxidation via electron delocalization in nickel hydroxide nanoribbon. Nat. Commun. **11**, 4647 (2020). https://doi.org/10.1038/s41467-020-18459-9
24. W.J. Huang, H.T. Wang, J.G. Zhou, J. Wang, P.N. Duchesne, D. Muir, P. Zhang, N. Han, F.P. Zhao, M. Zeng, J. Zhong, C.H. Jin, Y.G. Li, S.T. Lee, H.J. Dai, Highly active and durable methanol oxidation electrocatalyst based on the synergy of platinum–nickel hydroxide–graphene. Nat. Commun. **6**, 10035 (2015). https://doi.org/10.1038/ncomms10035
25. G.B. Melle, F.W. Hartl, H. Varela, E. Sitta, The effect of solution pH on the oscillatory electro-oxidation of methanol. J. Electroanal. Chem. **826**, 164–169 (2018). https://doi.org/10.1016/j.jelechem.2018.08.033
26. S. Ye, H. Kita, A. Aramata, Hydrogen and anion adsorption at platinum single crystal electrodes in phosphate solution over a wide range of pH. J. Electroanal. Chem. **333**, 299–312 (1992). https://doi.org/10.1016/0022-0728(92)80398-N
27. S.X. Leong, M. Carta, R. Malpass-Evans, N.B. McKeown, E. Madrid, F. Marken, One-step preparation of microporous Pd@cPIM composite catalyst film for triphasic electrocatalysis. Electrochem. Commun. **86**, 17–20 (2018). https://doi.org/10.1016/j.elecom.2017.11.007
28. M.N. Nasharudin, S.K. Kamarudin, U.A. Hasran, M.S. Masdar, Mass transfer and performance of membrane-less micro fuel cell: a review. Internat J. Hydrogen Energy. **39**, 1039–1055 (2014). https://doi.org/10.1016/j.ijhydene.2013.09.135
29. Y.Z. Zhao, R. Malpass-Evans, M. Carta, N.B. McKeown, P.J. Fletcher, G. Kociok-Kohn, D. Lednitzky, F. Marken, Size-selective photoelectrochemical reactions in microporous environments: Clark probe investigation of Pt@g-C_3N_4 embedded into intrinsically microporous polymer (PIM-1). ChemElectroChem 8, 3499–3505 (2021) http://doi10.1002/celc.202100732

Authors and Affiliations

Sirlon F. Blaskievicz[1,2] · Ivo F. Teixeira[1,3] · Lucia H. Mascaro[1] · Mariolino Carta[4] · Neil B. McKeown[5] · Yuanzhu Zhao[2] · Frank Marken[2]

✉ Frank Marken
f.marken@bath.ac.uk

[1] Department of Chemistry, Federal University of São Carlos, Zip Code 13565-905, São Carlos, SP, Brazil

[2] Department of Chemistry, University of Bath, Claverton Down, Bath BA2 7AY, UK

[3] Department of Colloid Chemistry, Research Campus Golm, Max-Planck Institute of Colloids and Interfaces, 14424 Potsdam, Germany

[4] Department of Chemistry, College of Science, Swansea University, Grove Building, Singleton Park, Swansea SA2 8PP, UK

[5] EaStCHEM, School of Chemistry, University of Edinburgh, Joseph Black Building, David Brewster Road, Edinburgh EH9 3JF, Scotland, UK